

# Knockdown of LCN2 Attenuates Brain Injury After Intracerebral Hemorrhage via Suppressing Pyroptosis

Yangyang Zhao<sup>1,\*</sup>, Qiuxiang Xiao<sup>2,\*</sup>, Tao Sun<sup>1</sup>, Haiyun Yu<sup>1</sup>, Muyun Luo<sup>3</sup>

<sup>1</sup>The First Clinical Medical College, Gannan Medical University, Ganzhou City, Jiangxi Province, People's Republic of China; <sup>2</sup>Department of Pathology, The First Affiliated Hospital of Gannan Medical University, Ganzhou City, Jiangxi Province, People's Republic of China; <sup>3</sup>Department of Neurosurgery, The First Affiliated Hospital of Gannan Medical University, Ganzhou City, Jiangxi Province, People's Republic of China

\*These authors contributed equally to this work

Correspondence: Muyun Luo, Department of Neurosurgery, The First Affiliated Hospital of Gannan Medical University, No. 23, Qingnian Road, Zhanggong District, Ganzhou City, Jiangxi Province, 341000, People's Republic of China, Tel +86- 13767715533, Email lmy771230@163.com

**Objective:** The aims of this study are to screen novel differentially expressed genes (DEGs) for intracerebral hemorrhage (ICH) and reveal the role of Lipocalin-2 (LCN2) in ICH.

**Methods:** We constructed the ICH model by injection of autologous whole blood into the right basal ganglia in rats. RNA-sequencing and bioinformatics analyses were performed to identify the DEGs between ICH and sham rats, and some important ones were confirmed using quantitative real-time PCR (qRT-PCR). LCN shRNA was used to knockdown of LCN2 in ICH rats. Pathological examination was carried out using 2,3,5-triphenyltetrazolium chloride (TTC) staining and Hematoxylin-eosin (HE) staining. Immunohistochemistry detected Caspase-3, and co-staining of Terminal dUTP nick end labeling (TUNEL) and NEUN staining were performed for neuron apoptosis assessment. Western blot analysis was performed to quantify pyroptosis-related proteins. Enzyme-linked immunosorbent assay (ELISA) was used to measure inflammatory cytokine levels.

**Results:** ICH rats exhibited significant hematomas, higher brain water content, obvious interstitial edema, and inflammatory infiltration, as well as more apoptotic cells in brain tissues. RNA-seq analysis identified 103 upregulated and 81 downregulated DEGs. The expression of LCN2, HSPB1, CXCL10, and MEF2B were upregulated in ICH rats. ICH triggered the release of interleukin (IL)-1 $\beta$ , tumor necrosis factor- $\alpha$  (TNF- $\alpha$ ), and IL-18, and promoted the expression of pyroptosis-related proteins Caspase-1, GSDMD, NLRP3, and ASC. LCN2 knockdown attenuated the pathological characteristics of ICH, and also reduced pyroptosis in brain tissues.

**Conclusion:** Inhibition of LCN2 attenuates brain injury after ICH via suppressing pyroptosis, which provide guidance for ICH management.

**Keywords:** intracerebral hemorrhage, pyroptosis, inflammation, lipocalin-2

## Introduction

Hemorrhagic stroke is a life-threatening bleeding disorder, accounting for 10–20% of strokes every year. Globally, the prevalence of this disorder is approximately 12–15% of cases per 100,000, and is still increasing mainly in Africans and Asians.<sup>1</sup> As a subtype of hemorrhagic stroke, intracerebral hemorrhage (ICH) is a non-traumatic spontaneous bleeding disorder with a high mortality and disability.<sup>2</sup> After ICH occurrence, the primary pathological injury is hematoma-induced mechanical compression to the brain, leading to brain hernia and brain edema, and subsequently inducing secondary brain injury including inflammation, oxidative stress, neuronal cytotoxicity, and thrombin formation.<sup>3</sup> Secondary brain injury has been recognized as a critical factor of cell death and neurological outcome after ICH. Although surgeries can be used to remove hematoma, secondary brain injuries remain huge challenges. Hence, it is urgent to develop promising strategies for brain injuries after ICH.

Pyroptosis, a pro-inflammatory programmed cell death modulated by the gasdermins (GSDMs) family, is unlike apoptosis and necrosis.<sup>4</sup> Pyroptosis plays important roles in many diseases, including cancer, liver disease, inflammatory diseases, and cardiovascular disease.<sup>5–8</sup> Notably, pyroptosis is implicated in the pathogenesis of neurological disorders, including cerebral ischemia/reperfusion injury, spinal cord injury, neurodegenerative disorders, and stroke.<sup>9,10</sup> It has been reported that polystyrene microplastic-induced ICH can result in secondary brain injury closely associated with inflammation and pyroptosis.<sup>11</sup> After ICH, the NOD-like receptor protein 3 (NLRP3)/Caspase-1/GSDMD signaling is crucial in pyroptosis, which further produces interleukin (IL)-1 $\beta$  and IL-18, as well as intracellular danger signals, resulting in the rupture and death of neurons, glial cells, or endothelial cells.<sup>4,12</sup> Inhibition of neuronal pyroptosis may alleviate neuroinflammation, reduce nerve injury<sup>13,14</sup> and improve functional outcomes after ICH.<sup>15</sup> Thereby, the inhibition of pyroptosis after ICH may offer a direction for ICH management.

Recently, with the help of transcriptomics and bioinformatics analysis, potential biomarkers have been identified to shed novel insights into pathological mechanisms of diverse diseases and provide promising therapeutic targets for treatment of diseases.<sup>16</sup> A previous study has screened 73 differentially expressed microRNAs that may reveal the mechanism of hyperglycemia in ICH mice. Further bioinformatics analyses deciphered that inhibition of the hedgehog signaling by these microRNAs deteriorates neurological function.<sup>17</sup> In this study, the RNA-Seq method accompanied by bioinformatics analysis was employed to screen novel differential expressed genes (DEGs) between ICH and sham rats. Lipocalin-2 (LCN2) was identified as a key DEG for ICH. LCN2, also known as neutrophil gelatinase-associated lipocalin, is a glycoprotein that transports small and hydrophobic molecules, and is commonly detected in several tissues such as the lung, heart, and kidney.<sup>18</sup> Compelling evidence have revealed that LCN2 is implicated in multiple biological processes, including inflammation, cell death, apoptosis, and cancer metastasis.<sup>19–21</sup> At present, LCN2 has been explored as a potential biomarker for renal injury, age-related brain diseases, vascular dementia, and Alzheimer's disease.<sup>18,22–24</sup> Importantly, LCN2 has been proven to be associated with secondary brain injury after cerebral stroke.<sup>25</sup> However, the role of LCN2 in pyroptosis after ICH-induced brain injury has not been confirmed. This study aimed to reveal the underlying mechanism of LCN2 in pyroptosis after ICH in rats.

## Methods

### Construction of ICH Model

A total of 90 Sprague-Dawley (SD) rats (320–360 g) were purchased from Beijing Huafukang Experimental Animal Co., Ltd. (Beijing, China) and kept in a stable environment at 22  $\pm$  2°C with free access to food and water. Experiments were performed in accordance with the guidelines of laboratory animal care and were approved by the Local Ethics Committee (Ethics number: LLSC-2021081901).

A total of 24 rats were divided into two groups: the control group (n = 12) and the ICH group (n = 12). SD rats were anesthetized intraperitoneally with 40 mg/kg of pentobarbital sodium. The induction of ICH model was performed using a semi-coagulated autologous whole blood model, as previously reported.<sup>26</sup> After complete anesthesia, animals were placed on the stereotactic instrument. A 1 mm burr hole was made in the skull (3.0 mm right lateral to the sagittal suture and 0.7 mm anterior to the bregma). A total of 60  $\mu$ L of autologous whole blood was then injected into the right basal ganglia slowly over 6 min at a depth of 5.0 mm with a microinfusion pump (Shanghai Alcott Biotech Co., Ltd., Shanghai, China). To prevent reflux and minimize tissue damage, the needle was slowly withdrawn 40 min after the injection. During the whole operation, the rats were placed supine on the heating blanket and maintained at a body temperature of 37  $\pm$  0.5°C. Rats in the sham group received the same operation without injection of autologous whole blood. Rats that died within 24 h after ICH were counted to determine the mortality rate.

### Brain Water Content Measurement

For brain water content measurement at different time points (24 h, 48 h, 72 h, and 96 h) after ICH model introduction, 30 rats were used (n = 6 for each group). Brain tissues were excised and immediately weighed (WW). Next, brain tissues were dried at 100°C for 24 h and weighed again (DW). The brain water content (%) was calculated according to [(WW – DW)/ WW]  $\times$  100.

## Knockdown of LCN2 in ICH Rats

For knockdown of LCN2 in ICH rats, a total of 36 rats were assigned into 3 group ( $n = 12$  for each group). Lentivirus-mediated shRNA silencing methods were employed for knockdown of LCN2 in ICH rats. Lentiviruses were generated in 293T cells using second generation packaging vectors by Genomeditech Co., Ltd. (Shanghai, China). LCN2 short hairpin RNA (shRNA) oligonucleotides were cloned into a lentiviral vector (LV-shLCN2) and then synthesized by Genomeditech Co., Ltd. Its corresponding control lentivirus served as LV-NC. Individual clones were identified by their unique TRC number: TRCN0000060289 (CCAGCATGCTATGGTGTCTT) for shLCN2 (289) and TRCN0000060290 (GTACTTCAAGATCACCTCTA) for shLCN2 (290); TRCN0000072246 (CAAATCACAGAATCGTCGTAT) for vector control. Afterwards, 4  $\mu\text{L}$  of LV-shLCN2 lentivirus or LV-NC lentivirus was injected into the right lateral cerebral cortex motor area of the ICH rats by using a 5- $\mu\text{L}$  Hamilton syringe at a rate of 1  $\mu\text{L}/\text{min}$ .<sup>27</sup> Neurobehavioral deficits were examined at 72 h after injection. Subsequently, blood samples were obtained from rats. After being euthanized by cervical dislocation, brain tissues were excised from all rats and washed by cold phosphate-buffered saline (PBS). Blood samples and other brain tissues were frozen in liquid nitrogen and stored in  $-80^{\circ}\text{C}$ .

## Behavioral Analysis

Short-term neurological functions were evaluated using the modified Garcia test and Beam balance test as previously reported<sup>28</sup> at 24 h after ICH or 72 h after shRNA injection. The modified Garcia test included 6 subtests such as spontaneous activity (3 min), side stroking, vibrissae touch, limb extension, forepaw outstretching, and climbing (1 min); For the Beam balance test, rats were placed on the platform (at both ends of a 1.5-cm round rod) for 30s. Next, they were placed perpendicular to the center of the rod and given 1 min to pass through the beam. Two trained investigators, blinded to experimental groups, evaluated the neurobehavioral deficits.

## 2, 3, 5-Triphenyltetrazolium Chloride (TTC) Staining

To examine the outcomes of brain tissue, 3 sham rats and 3 ICH rats were euthanized at 24 h after ICH or 72 h after shRNA injection. Fresh brain tissues were excised immediately, and then brain tissues were stained with TTC (Sigma, USA) for 30 min to measure changes of hemorrhage after ICH induction or shLCN2 injection.

## Hematoxylin-Eosin (HE) Staining

Tissues from the hematoma area of the right basal ganglia area are collected for pathological examination. Part of brain tissues were fixed with 10% formaldehyde (Solarbio, Beijing, China) for 10 min and embedded in paraffin. Slides, 4  $\mu\text{m}$  thick, were cut, deparaffinated with xylene, and rehydrated with descending concentration of ethanol (100%, 96%, 80%, 70%, and 50% for 2 min, respectively). Afterwards, slides were stained with hematoxylin solution (Servicebio, Wuhan, China) for 5 min and in hydrochloric acid-ethanol mixtures for 3s, followed by washing for 15 min. Slides were stained with 0.5% eosin solution (Servicebio) for 1 min. Slides were treated with 80%, 95% and 100% alcohol for 2 min respectively, and dehydrated with xylene for 2 min. Pathological examination was performed under a microscope (Nikon, Japan). Three rats were examined per group. Five visual fields were randomly selected from the hematoma area of the right basal ganglia area for each slide.

## Immunohistochemistry

The paraffin-embedded slides were dewaxed with xylene and rehydrated with descending concentrations of ethanol. A 10 mmol/L sodium citrate solution was prepared for antigen retrieval for 6 min and then placed at room temperature for 1 h. Slides were washed with PBST for 5 min and incubated with 0.3%  $\text{H}_2\text{O}_2$ /methanol solution for 30 min at  $4^{\circ}\text{C}$  to inactivate endogenous peroxidase activity, and then blocked using 3% bovine serum albumin (Ausbian, Australia). Subsequently, slides were incubated with a primary antibody against Caspase-3 (Abcam, UK; 1:100) overnight at  $4^{\circ}\text{C}$  and then incubated with horseradish peroxidase-linked streptavidin (Thermo Fisher) for 80 min. After washing with PBS, color was developed by a mixture of 85% double distilled water +5% 3,3'-diaminobenzidine (DAB), 5% DAB substrate +5% DAB chromogen for 3 min (DAB substrate kit; Thermo Fisher). Next, slides were stained with hematoxylin

solution (Servicebio) for 5 min and coverslipped with resin. Three rats were examined per group, and five visual fields were randomly selected from the hematoma area of the right basal ganglia area for each slide. Positive Caspase-3 staining was observed under a light microscopy, and the brown chromogen at the edge of the hematoxylin-stained cell nuclei and in the cytoplasm or plasma membrane of the cells was considered as positive staining.

## Apoptotic Neurons Staining

To evaluate the neuronal apoptosis, co-staining of neuronal apoptosis was conducted by NEUN staining and TUNEL staining. Slides were incubated with mouse anti-NEUN antibody (1:100, Abcam, UK) overnight at 4°C. TUNEL staining was conducted using Apoptosis Detection Kit (Roche, USA) as recommended by the manufacturers at 24 h after ICH. 4',6-diamidino-2-phenylindole (DAPI) solution was used to label nuclei with blue fluorescence at 4°C. Apoptosis was observed under a fluorescence microscope (Zeiss, Germany). Three rats were examined per group and five visual fields were randomly selected from the hematoma area of the right basal ganglia area for each slide. The number of positive cells were counted using a cell-counter (Olympus, Japan). The positive neurons were identified by red cells (TUNEL) located in green neurons (NEUN) with a blue nucleus (DAPI). Data was expressed as ratio of positive neurons (%).

## RNA-Sequencing Transcriptome Analysis

Total RNA was obtained by Trizol reagent (Thermo Fisher) from brain tissues of sham (n = 3) and ICH rats (n = 3). The quality and concentration of RNA were evaluated by Nano-100 (Aosheng Instrument Co., LTD, Hangzhou, China). RNA samples with RIN > 7.0 were selected for sequencing library construction. Afterward, mRNA was purified from 5 µg total RNA using Dynabeads Oligo (dT) (Thermo Fisher), and split into short fragments by divalent cations at 94°C for 6 min, which were subsequently transcribed into cDNA using FastKing gDNA Dispelling RT SuperMix kit (TianGen Biotech, China). U-labeled second-stranded DNAs were generated using E. coli DNA polymerase I (NEB, USA), RNase H (NEB, USA), and dUTP Solution (Thermo Fisher). A SYBR Green kit (TianGen Biotech) was employed for PCR on a BIO-RAD C1000 Touch Thermal Cycler PCR system (Bio-Rad Laboratories, Inc.). The 2 × 150 bp paired-end sequencing was carried out on Illumina Novaseq™ 6000 (LC-Bio Technology CO., Ltd., Hangzhou, China). Raw reads containing adapters or low-quality bases were trimmed with Cutadapt (<https://code.google.com/p/cutadapt/>) with a Phred quality cutoff of 20, and reassessed with FastQC. DESeq2 software was utilized to screen DEGs. Genes with  $|\log_2\text{FoldChange}| > 1$  and  $P\text{-value} < 0.05$  were defined as DEGs. Moreover, the volcano plots of DEGs were drawn using the ggplots2 package in R software (version 4.2.1). Complete-Linkage method was used for hierarchical clustering analysis of DEGs between the two groups, and the heatmap was visualized using the Pheatmap R package.

## Functional Enrichment Analysis

DEGs between the sham and ICH groups rats were used for GO and KEGG pathway enrichment analyses based on CluGO 19 in Cytoscape (<https://cytoscape.org/>). The GO functional enrichment included biological process (BP), cellular component (CC) and molecular function (MF) categories.

## Quantitative Real-Time PCR (qRT-PCR)

After extracting the total RNAs from brain tissues of sham (n = 6) and ICH rats (n = 6) using TRIzol (Thermo Fisher), the quality and concentration of RNA were evaluated using 2 µL RNA on Nano-100 (Aosheng Instrument Co., LTD). 1 µg of extracted RNA was reverse transcribed to cDNA using Hiscript II QRT Supermix for qPCR kit (Vazyme, China). A ChamQ Universal SYBR kit (Vazyme) was implemented for RT-qPCR using 25 ng of cDNA on the QPCR Mx3005P system (Agilent Technologies Stratagene) with the thermocycler conditions: initial denaturation at 95°C for 30s, 40 cycles of denaturation at 95°C for 10s, annealing at 60°C for 30s, followed by 95°C for 15s, 60°C for 60s, and 95°C for 15s. GAPDH was used as an internal control. The relative expression was calculated using a  $2^{-\Delta\Delta CT}$  method. Table 1 details the primers sequences for qPCR.

**Table 1** Primers Sequences for RT-qPCR

Primer Name	Sequence (5'-3')
R-GAPDH-F	CTCATGACCACAGTCCATGC
R-GAPDH-R	TTCAGCTCTGGGATGACCTT
R-CXCL10-F	GATGCAGTTAATGCCCCACT
R-CXCL10-R	TTCCTTATTGGGGTCAGCAC
R-MEF2B-F	TGACGGAGATCACAGTCTGG
R-MEF2B-R	GAGCTGTAAACGGCGGAGTA
R-HSPB1-F	GTGGGTGGAAAGGAGAACAA
R-HSPB1-R	GGCCAATCTGTAGGAGTCCA
R-LCN2-F	TGACAGTAGGCAGCATGGAG
R-LCN2-R	GTAATGGGCGAACTTGCATT
NLRP3-F	ATGCTGCTTCGACATCTCCT
NLRP3-R	AACCAATGCGAGATCCTGAC
GSDMD-F	TGCGTGTGACTCAGAAGACC
GSDMD-R	ATAAAGCTCCAGGCAGCGTA
Caspase-1-F	CACAGCTCTGGAGATGGTGA
Caspase-1-R	TCTTTCAAGCTTGGGCACTT
ASC-F	CAGGCTCTAATGGCTGCTTC
ASC-R	ATGCGACATTTGACATGGAA

## Western Blot

Six brain tissues from each group were ground into tissue homogenate on ice, and total protein was obtained with the ProteoPrep<sup>®</sup> Total Extraction Sample kit (Sigma). Equal quantities of protein (6  $\mu$ L) were separated on 10% SDS-PAGE and transferred onto 0.2  $\mu$ m PVDF membranes for 60 min, which were blocked in 5% skim milk for 2 h at room temperature. Next, membranes were incubated with primary antibodies against LCN2 (Abcam, 1:1000), Caspase-1 (Abcam, 1:1000), GSDMD (Abcam, 1:1000), NLRP3 (Abcam, 1:1000), and ASC (Abcam, 1:1000) overnight at 4°C. Next, HRP-labeled goat anti-rabbit IgG (Abcam, 1:5000) was applied for 1 h at room temperature. Blots were visualized using ECL on a Tanon 5200 chemiluminescence imaging system.

## ELISA

Six serum samples from each group were obtained after centrifugation at 4000 rpm for 15 min. The levels of TNF- $\alpha$ , IL-1 $\beta$ , and IL-18 in the serum were measured by ELISA kits (Beyotime, Shanghai, China) following the manufacturer's protocol. The antibodies against TNF- $\alpha$ , IL-1 $\beta$ , and IL-18 were added in 96-well plates and incubated for 1 min at 37°C. Subsequently, 100  $\mu$ L horseradish peroxidase-labelled antibodies were added to each well and incubated for 60 min at 37°C. 50 mL of 2.5 M sulfuric acid was added for 15 min to stop the reaction, and the absorbance was read at 450 nm using a microplate reader (DynaTech, New York, USA).

## Measurement of Lactate Dehydrogenase (LDH) Release

Serum samples were collected from each group. LDH content was measured using the LDH Cytotoxicity Assay Kit (Abcam) following the manufacturer's instructions to detect pyroptotic cell death.

## Caspase-1 Activity Analysis

Serum samples were collected, and Caspase-1 activity was assessed using the Caspase-1 activity assay kit (Bosterbio, Pleasanton, California, USA) in accordance with the manufacturer's instructions.

## Statistics

All experimental data were processed using GraphPad Prism 7.0 software (GraphPad Prism Software Inc., San Diego, California) and expressed means  $\pm$  SD. Comparisons among multiple groups were performed using one-way ANOVA or

two-way ANOVA, followed by Tukey's multiple comparisons test. Differences between two groups were compared using *t*-tests.  $P < 0.05$  was considered as statistically significant.

## Results

### ICH Model is Successfully Established

Firstly, we evaluated the mortality rate of rats after 24 h for ICH construction. The findings indicated that there were 2 fatalities, both in the ICH group, resulting in an approximate mortality rate of 8%. After successfully establishment of ICH model in rats, the brain tissues of ICH and sham rats were excised and the brain injury was subsequently examined. As shown in **Figure 1A**, the brain tissue in ICH model was slightly atrophied and deformed, and obvious hematomas was observed at the hemorrhage site compared with sham rats. Next, the results showed that ICH rats had significant higher brain water content than that of sham rats, especially at 72 h after ICH ( $P < 0.0001$ ) (**Figure 1B**). **Figure 1C** and **D** displayed that ICH rats exhibited reduced modified Garcia score and Beam balance score than that of sham ( $P < 0.0001$ ), indicating a poor behavioral function after ICH. Further pathological examination using HE staining displayed that sham rats exhibited normal brain tissue structure and clear cell layer; brain cells were arranged orderly without interstitial edema and inflammatory infiltration. While, compared with the sham group, ICH rats showed obvious interstitial edema, increased inflammatory cells, and slightly disordered cells (**Figure 1E**). Additionally, the positive Caspase-3 cells were remarkably increased in brain tissue of ICH rats detected by immunohistochemistry (**Figure 1F**). Similarly, co-staining of TUNEL and NEUN staining found more apoptotic neurons in brain tissue of ICH rats than that of sham rats ( $P < 0.0001$ ) (**Figure 1G**).

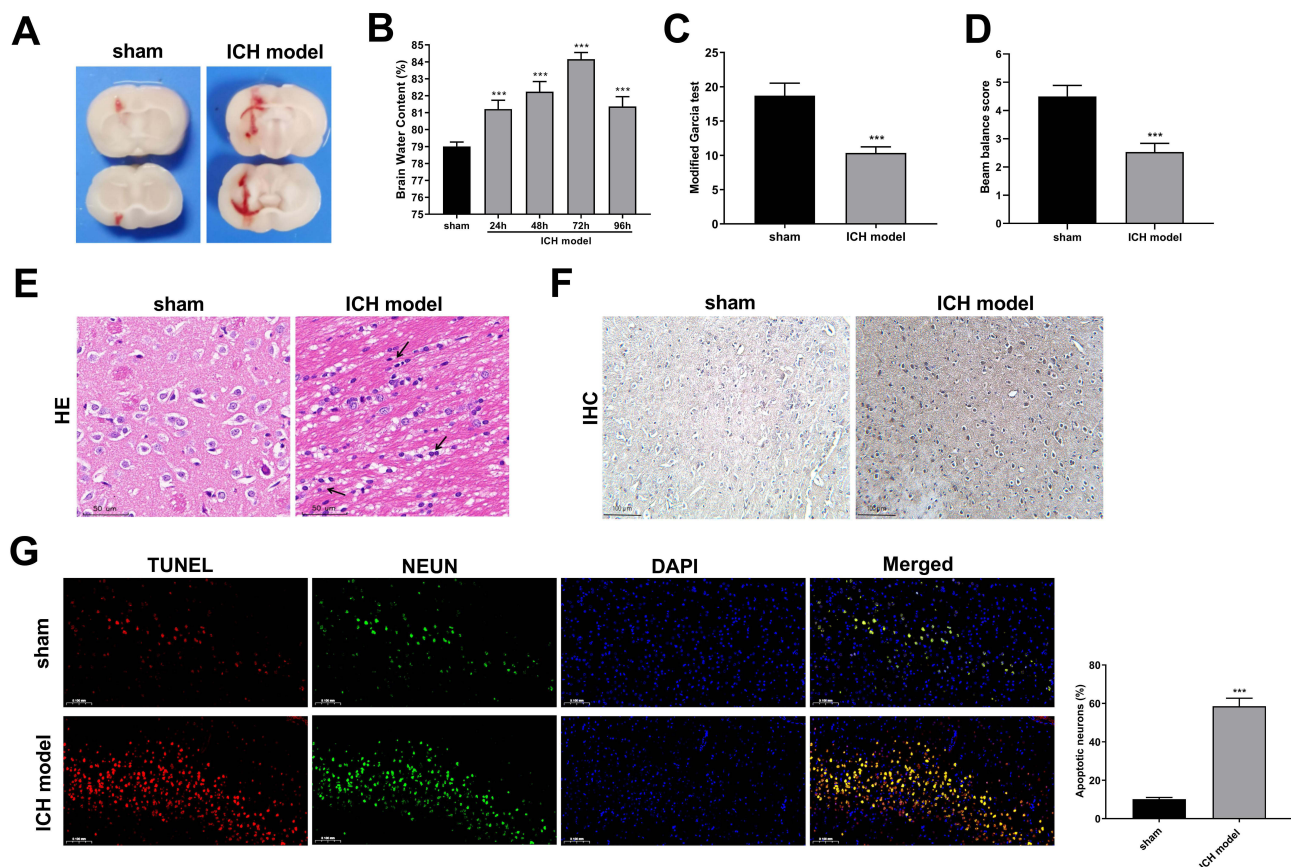


**Figure 1** A rat model of intracerebral hemorrhage is successfully established.

**Notes:** (A) TTC staining evaluates hemorrhage size in brain tissues of ICH and sham rats. (B) The brain water content in ICH and sham rats at 24, 48, 72 and 96 h after hemorrhage. (C and D) Neurobehavioral evaluation using modified Garcia score and Beam balance score after ICH. (E) Pathological examination of brain injury using HE staining (magnification 20 $\times$ ). Arrows indicate inflammatory cells. (F) Immunohistochemistry measured Caspase-3 positive cells in ICH and sham rats (Scale bar: 100  $\mu$ m; magnification 20 $\times$ ). Caspase-3 positive staining is located in the cytoplasm and manifests as a brown sediment in immunostaining. (G) Co-staining of TUNEL and NEUN for measurement of apoptotic neurons in brain tissues of ICH and sham rats. (magnification 20 $\times$ ). \*\*\* $P < 0.0001$ , versus sham group.

## Identification of DEGs Between ICH and Sham Rats

Subsequently, brain tissues of ICH and sham rats were collected for transcriptome sequencing. Candidates with  $|\log_2\text{FoldChange}| > 1$  and  $P\text{-value} < 0.05$  were considered as DEGs. Bioinformatics analysis found that the expression profiles were significantly altered between ICH and sham rats. **Figure 2A** portrayed a distinct clustering of DEGs between ICH and sham rats. Totally, 184 DEGs were screened, including 103 upregulated genes and 81 downregulated genes (**Figure 2B**). **Table 2** listed the top 20 DEGs between ICH and sham rats.

## Functional Enrichment Analysis

To understand the biological process of DEGs, KEGG and GO enrichment analyses were further performed. **Figure 3A** displayed the most significant top 10 GO items. DEGs were mainly enriched in extracellular region and extracellular space in CC category. For MF category, receptor ligand activity, cell adhesion molecule binding, and signaling receptor activator activity were significantly enriched. For BP category, DEGs were significantly enriched in response to external stimulus and regulation of multicellular organismal process. Meanwhile, the results from KEGG enrichment analysis showed that DEGs were enriched in DNA replication, primary immunodeficiency, TNF signaling pathway, and MAPK signaling pathway (**Figure 3B**). The results indicated that ICH affected the transcription process and some signal transduction pathways.

## Validation of DEGs Using RT-qPCR

Furthermore, the expression levels of LCN2, HSPB1, CXCL10, and MEF2B were measured in brain tissues by RT-qPCR. As displayed in **Figure 4**, LCN2 ( $P = 0.0029$ ), HSPB1 ( $P < 0.0001$ ), CXCL10 ( $P = 0.0005$ ) and MEF2B ( $P = 0.0057$ ) were significantly upregulated in ICH rats compared with sham. These results were consistent with that of RNA-sequencing.

## ICH Induces Pyroptosis in Brain Tissues

To clarify the role of pyroptosis in ICH, the pro-inflammatory cytokines (TNF- $\alpha$ , IL-1 $\beta$ , and IL-18) were also detected by ELISA, and the results revealed that TNF- $\alpha$ , IL-1 $\beta$ , and IL-18 were highly expressed in brain tissues of ICH rats ( $P < 0.0001$ ).

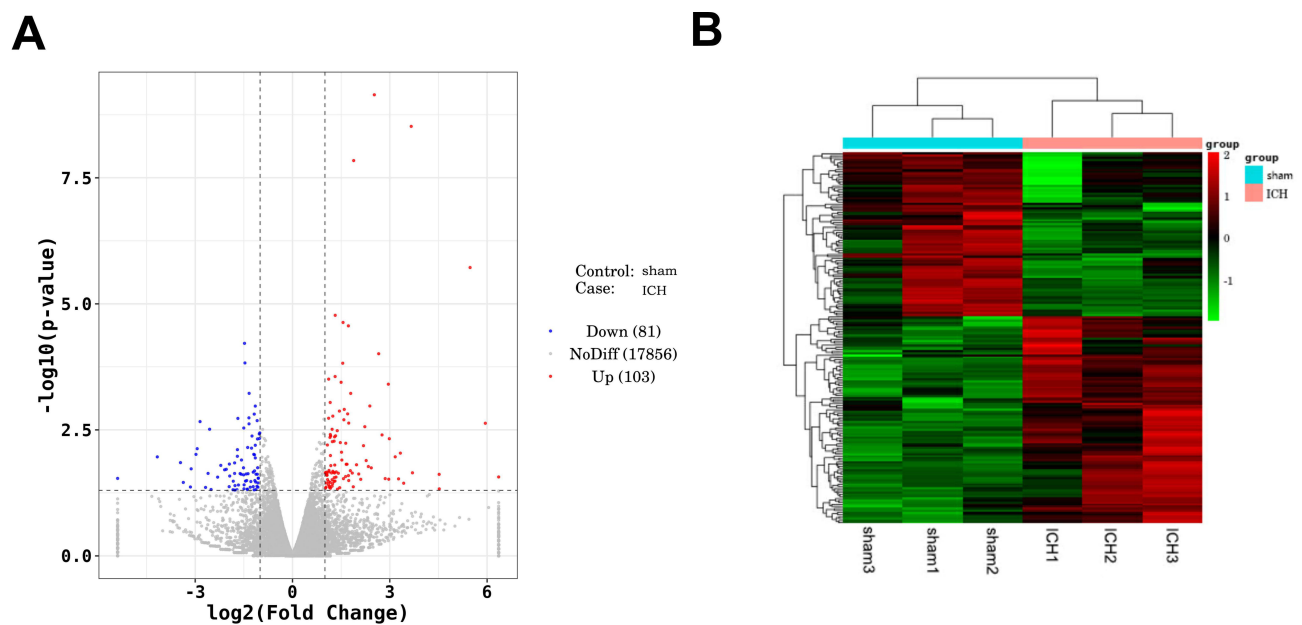


**Figure 2** Identification of DEGs between ICH and sham rats.

**Notes:** (A) Volcano diagram of DEGs between ICH group and sham rats. Red dots represent up-regulated DEGs, the blue ones represent down-regulated DEGs, and the gray dots represent the DEGs without significant differences. (B) The cluster heatmap of DEGs between ICH group and sham rats. Red represents up-regulated DEGs, and green represents down-regulated DEGs.

**Table 2** Top 20 DEGs Between ICH and Sham Rats

Genes	Description	Pval	Up/Down
LOC299282	Serine protease inhibitor	0.002	Up
LCN2	Lipocalin 2	1.90E-06	Up
MEF2B	Myocyte enhancer factor 2B	0.024	Up
CXCL10	C-X-C motif chemokine ligand 10	0.022	Up
CSF2RB	Colony stimulating factor 2 receptor beta common subunit	3.02E-09	Up
TACSTD2	Tumor-associated calcium signal transducer 2	0.036	Up
TIMP1	TIMP metalloproteinase inhibitor 1	0.009	Up
CD300E	Cd300e molecule	0.03	Up
HSPB1	Heat shock protein family B	0.011	Up
SP5	Sp5 transcription factor	0.005	Up
LNPI	Leukemia NUP98 fusion partner 1	0.029	Down
ANO2	Anoctamin 2	0.011	Down
NKX2-1	NK2 homeobox 1	0.014	Down
SLC9A2	Solute carrier family 9 member A2	0.035	Down
KRT77	Keratin 77	0.043	Down
SCN5A	Sodium voltage-gated channel alpha subunit 5	0.019	Down
KRT71	Keratin 71	0.010	Down
FSD2	Fibronectin type III and SPRY domain containing 2	0.007	Down
B9D1	B9 domain containing 1	0.002	Down
NTF3	Neurotrophin 3	0.044	Down

(Figure 5A). Additionally, there was a significant increase in LDH content and Caspase-1 activity in the ICH model group compared to the sham group ( $P < 0.0001$ ; Figure 5B and C). The levels of pyroptosis-related genes Caspase-1, GSDMD, NLRP3, and ASC were then determined using RT-qPCR. In brain tissues of ICH rats, the expression of Caspase-1 ( $P < 0.0001$ ), GSDMD ( $P = 0.0023$ ), NLRP3 ( $P < 0.0001$ ), and ASC ( $P < 0.0001$ ) were distinctly higher than that of sham rats (Figure 5D). Meanwhile, similarly, Western blot analysis showed that Caspase-1 ( $P = 0.0038$ ), GSDMD ( $P = 0.0055$ ), NLRP3 ( $P = 0.0053$ ), and ASC ( $P < 0.0050$ ) were significantly overexpressed compared with the sham group (Figure 5E). These findings suggested that ICH provoked pyroptosis in brain tissues of rats.

## Knockdown of LCN2 Attenuates ICH in Rats

LCN2 has been showed to be associated with brain injury after cerebral stroke and is involved in neuroinflammation after ICH. Based on the results of RNA-seq and further validation, LCN2 was identified as an upregulated DEGs between ICH and sham rats. Therefore, LCN2 was selected in this study for further mechanistic investigation. To evaluate the regulatory role of LCN2 in ICH, LCN2 was further silenced. Western blot analysis was utilized to confirm the knockdown effectiveness. As displayed in Figure 6A, the protein level of LCN2 was downregulated in the Lv-LCN2 group compared with the Lv-NC group ( $P = 0.0114$ ). After knockdown of LCN2 in ICH rats, hematomas were remarkably alleviated in the Lv-LCN2 group compared with the Lv-NC group (Figure 6B). Besides, the brain water content decreased by approximately 2% in the Lv-LCN2 group compared with the Lv-NC group at 72 h ( $P = 0.0067$ ) (Figure 6C). Also, knockdown of LCN2 could improve the ICH-induced poor modified Garcia score ( $P = 0.0037$ ) and Beam balance score ( $P = 0.0026$ ) (Figure 6D and E). Pathological examination revealed that knockdown of LCN2 attenuated interstitial edema, inflammatory infiltrations, and slightly disordered cells in ICH rats (Figure 6F). TUNEL staining also demonstrated that knockdown of LCN2 apparently reversed ICH-induced neurons apoptosis ( $P < 0.0001$ ) (Figure 6G). Collectively, knockdown of LCN2 could attenuate ICH in rats.

## Knockdown of LCN2 Suppresses Pyroptosis in ICH Rats

Knockdown of LCN2 could inhibit TNF- $\alpha$  ( $P = 0.0014$ ), IL-1 $\beta$ , and IL-18 secretion ( $P < 0.0001$ ) compared with the Lv-NC group (Figure 7A). LCN2 knockdown reduced LDH content and Caspase-1 activity ( $P < 0.0001$ ; Figure 7B and C).

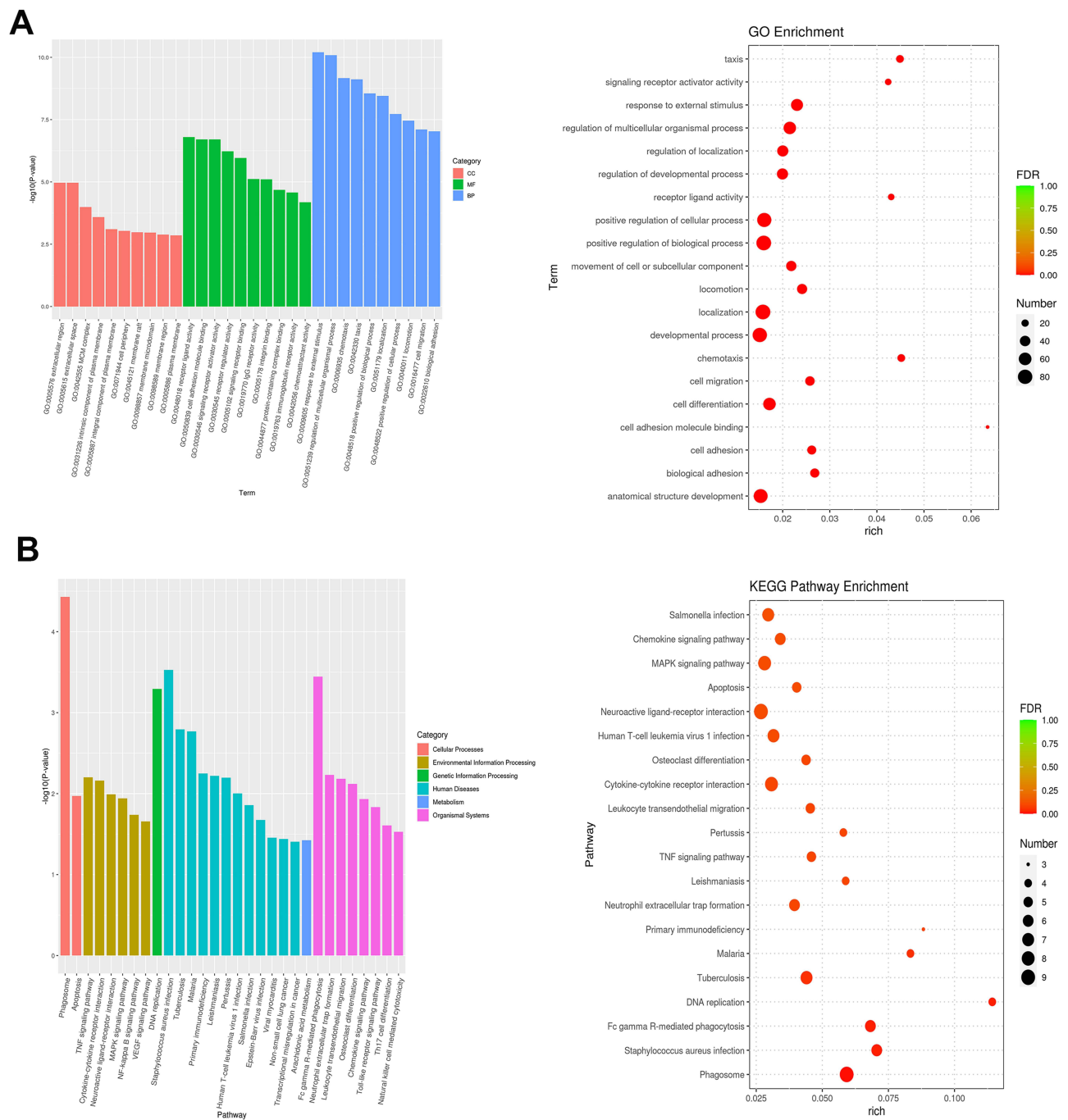


**Figure 3** Functional enrichment analyses of DEGs. **Notes:** (A) Histogram and bubble chart showing GO terms for BP, CC and MF categories. (B) Histogram and bubble chart showing the results of KEGG analysis.

Additionally, Western blot confirmed that knockdown of LCN2 significantly suppressed Caspase-1 ( $P = 0.0012$ ), GSDMD ( $P = 0.0254$ ), NLRP3 ( $P = 0.0033$ ), and ASC ( $P = 0.0027$ ) compared with the Lv-NC group (Figure 7D). These results indicated that knockdown of LCN2 could attenuate ICH through suppressing pyroptosis in rats.

## Discussion

With the application of large-scale sequencing, studies focusing on disease biomarkers gradually became an attractive and promising field in disease management. In this study, ICH model was constructed by injection of autologous whole

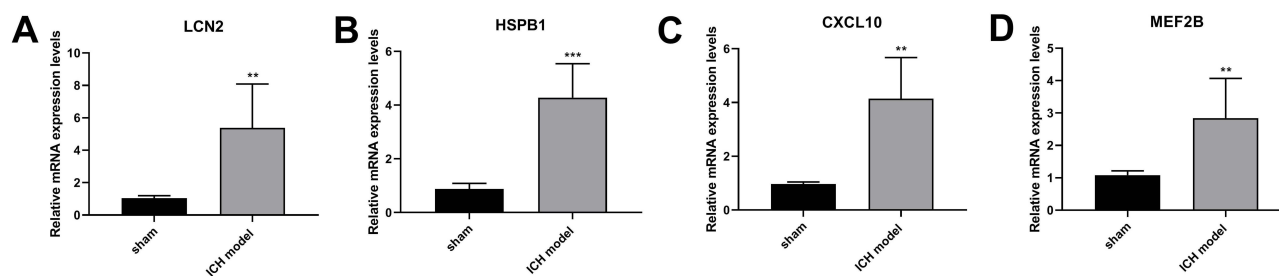


**Figure 4** Validation of DEGs using RT-qPCR.

**Notes:** Upregulation of LCN2 (A), HSPB1 (B), CXCL10 (C), and MEF2B (D) in brain tissues of ICH rats. \*\* $P < 0.01$  and \*\*\* $P < 0.0001$ , versus sham group.

blood into the right basal ganglia. Based on RNA-sequencing transcriptome analysis and bioinformatics analysis, 184 DEGs were identified between ICH and sham rats, and LCN2 ranked as the second DEG, which provided a evidence for the selection of LCN2 for further experiments. Further studies demonstrated that ICH induced pyroptosis in brain tissues, whereas knockdown of LCN2 could attenuate ICH in rats via inhibiting pyroptosis. This study first confirmed the role of LCN2 in pyroptosis after ICH-induced brain injury. This study might provide a potential direction of management for ICH from the perspective of pyroptosis.

After ICH-induced hematoma occurrence, brain injury was caused by immune infiltration and release of inflammatory cytokines, leading to the dysfunction of blood-brain barrier, formation of edema, as well as resulting in cell death.<sup>29</sup> It has been reported that HO-1, TNF- $\alpha$ , and IL-1 $\beta$  were significantly altered in brain tissues surrounding hematoma at 6–24 h and 24–72 h after ICH. Another study has demonstrated that neuronal apoptosis after ICH is induced by Toll-like receptor 4-mediated inflammatory responses, whereas it can be remarkably prevented with the injection of IL-1 $\beta$  and TNF- $\alpha$  antagonists in mice.<sup>30</sup> These findings imply that inhibition of inflammatory responses is of great significance in alleviating brain injury after ICH.<sup>31</sup> Additionally, a recent study has confirmed that the release of IL-1 $\beta$  and TNF- $\alpha$  results in activation of microglial cells and inflammatory responses, however, suppression of the crosstalk between NOD1/RIP2 and IL-1 $\beta$ /TNF- $\alpha$  inactivates microglial cells and inhibits neuronal inflammatory reactions.<sup>32</sup> In this study, the results from ELISA showed that pro-inflammatory cytokines TNF- $\alpha$ , IL-1 $\beta$ , and IL-18 were significantly increased in brain tissues after ICH in rats, indicating that increased TNF- $\alpha$ , IL-1 $\beta$ , and IL-18 might contribute to ICH-induced brain injury.

It has been reported that ICH not only induces significant inflammatory infiltration but also triggers the activation of ASC-NLRP3-GSDMD signaling leading to pyroptosis, which is associated with brain injury after ICH.<sup>11</sup> Increased intracranial pressure promotes the accumulation of Caspase-1, GSDMD-N, IL-1 $\beta$ , and IL-18 through triggering NLRP3 inflammasome in microglial cells after ischemia in rats.<sup>33</sup> NLRP3 inflammasome is crucial for the innate immunity and promotes production of caspase-1 and IL-1 $\beta$ , which aggravate inflammation after ICH.<sup>34</sup> Liang et al found that eliminating Caspase-1 remarkably improves blood–brain barrier permeability and integrity via the inactivation of pyroptosis after ischemic cerebral infarction.<sup>35</sup> Recently, Gu et al have revealed that Raf kinase inhibitor protein (RKIP) could reduce brain water content, improve blood–brain barrier and decrease hematoma after ICH. Besides, the activation of RKIP attenuates brain injury by suppressing pyroptosis-associated proteins, including NLRP3, Caspase-1, and GSDMD-N.<sup>36</sup> This study deciphered that pyroptosis-related genes such as Caspase-1, GSDMD, and NLRP were highly expressed in brain tissues of ICH rats, implying that ICH induced pyroptosis in ICH rats.

In the present study, transcriptome sequencing was performed in brain tissues of ICH and sham rats and 184 DEGs containing 103 significantly upregulated genes and 81 downregulated genes were identified. Functional enrichment analysis revealed that these DEGs were significantly enriched in DNA replication, primary immunodeficiency, TNF signaling pathway, and MAPK signaling pathway. Liu et al have demonstrated that 10 hub genes were identified and significantly enriched in TNF signaling pathway, which may be implicated in the pathological process of ICH and affect the prognosis via regulation of KEGG pathway.<sup>37</sup> Neuroinflammation is induced after ICH mainly through MAPK-mediated inflammatory responses, while inhibition of JNK and p38 MAPK signaling pathway attenuates neuroinflammation.<sup>38</sup> Traditional Chinese Medicine Liangxue Tongyu Formula has been proven to alleviate ICH-induced stroke through MAPK signaling pathway, TNF signaling pathway, calcium, and apoptosis, which indicates

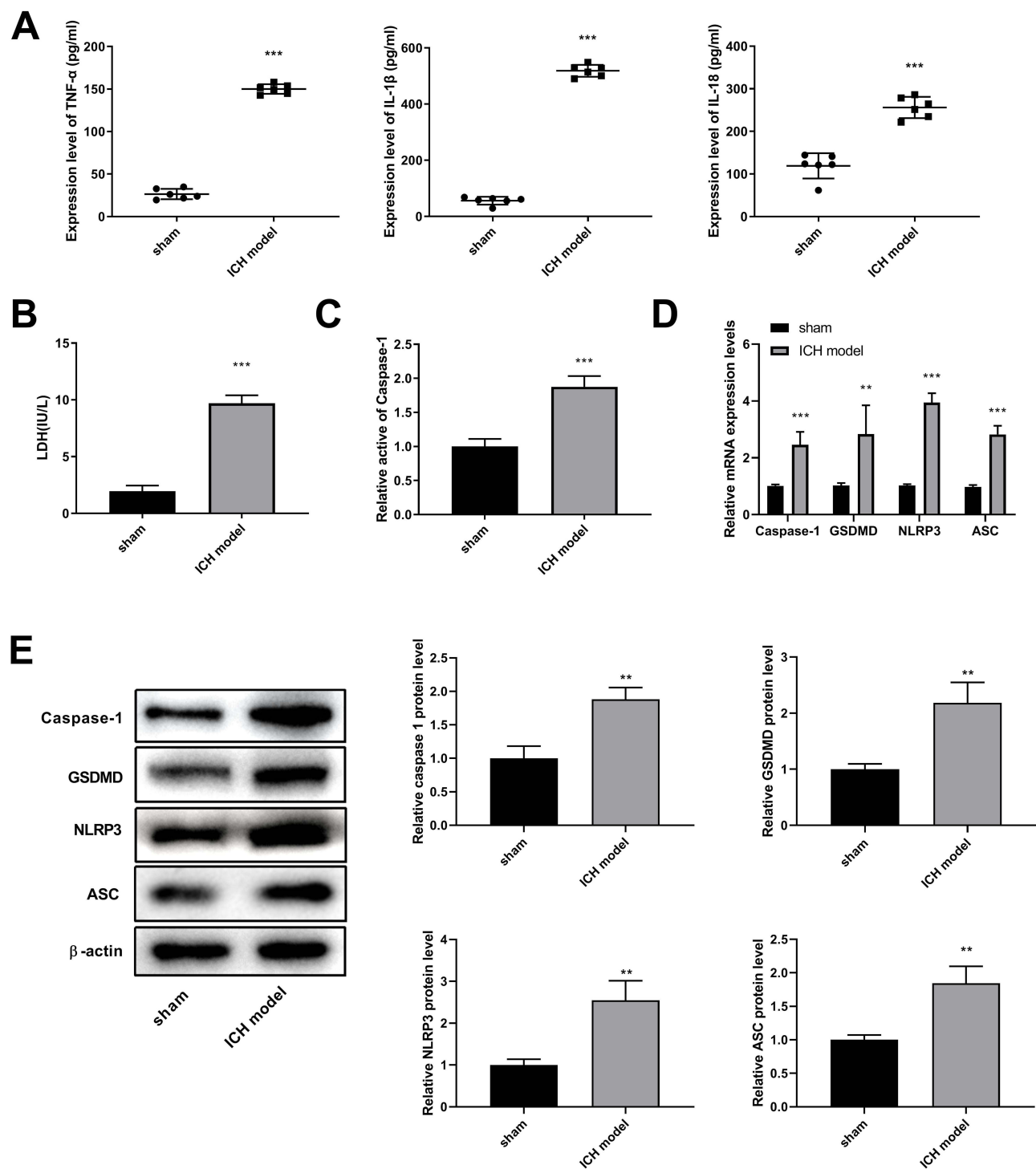


**Figure 5** ICH induces pyroptosis in brain tissues.

**Notes:** (A) The expression levels of pro-inflammatory cytokines TNF- $\alpha$ , IL-1 $\beta$ , and IL-18 in brain tissues of ICH rats measured by ELISA. (B) LDH content was assessed in the sham and ICH model groups. (C) Caspase-1 activity evaluation in the sham and ICH model groups. (D) The relative mRNA expression levels of Caspase-1, GSDMD, NLRP3, and ASC in brain tissues of ICH rats. (E) Western blot analysis was performed to quantify Caspase-1, GSDMD, NLRP3, and ASC. \*\* $P < 0.01$  and \*\*\* $P < 0.0001$ , versus sham group.

that MAPK signaling pathway and TNF signaling pathway may contribute to ICH-induced stroke, whereas regulation of these pathways provides promising strategy for ICH management.<sup>39</sup> As a result, we speculated that neuroinflammation was induced after ICH, probably through TNF and MAPK-mediated inflammatory responses.

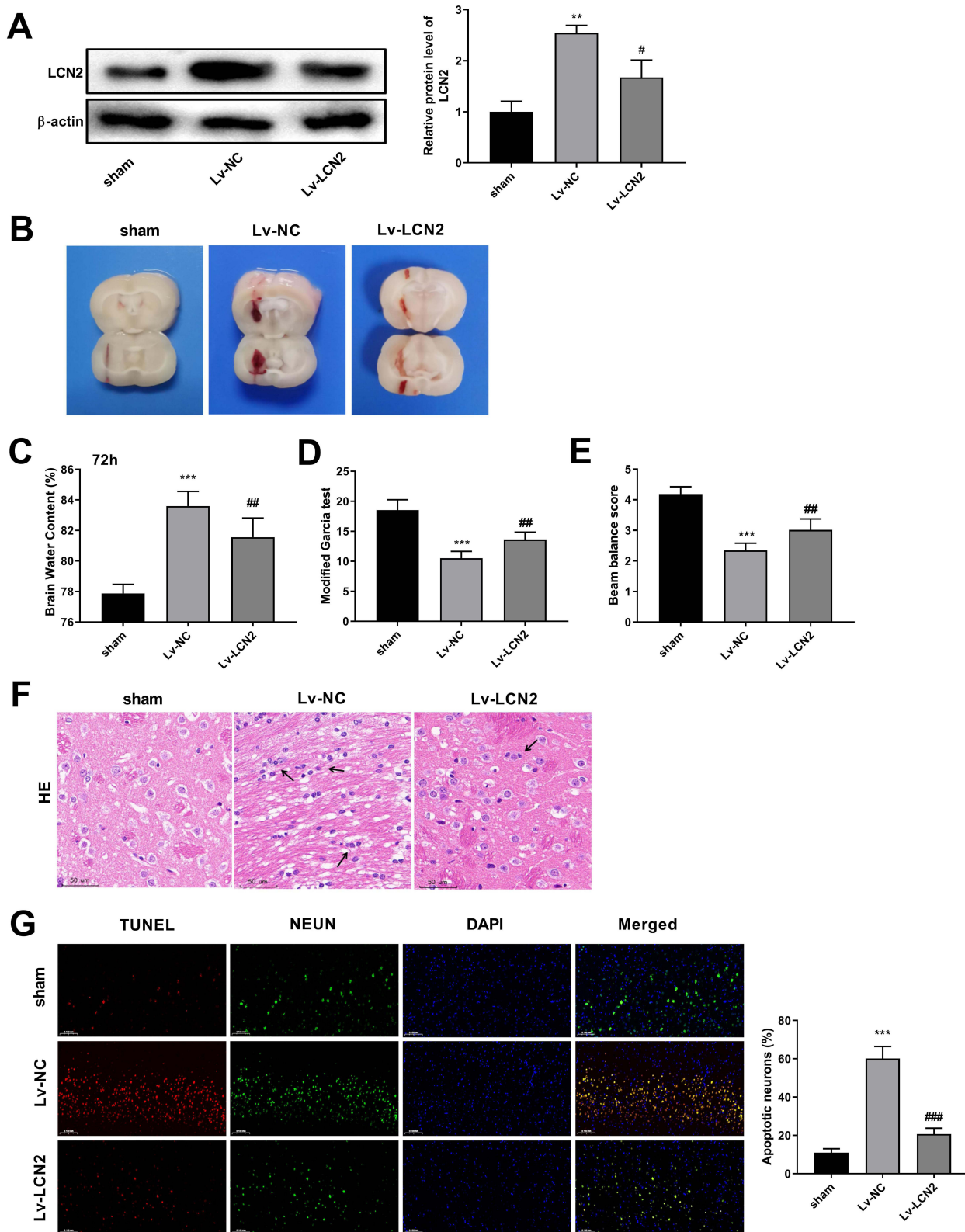


**Figure 6** Knockdown of LCN2 attenuates ICH in rats.

**Notes:** (A) Knockdown effectiveness is determined by Western blot analysis after injection of Lv-LCN2. (B) TTC staining evaluates changes of hemorrhage size in brain tissues after knockdown of LCN2. (C) The brain water content in ICH rats at 72h after injection of Lv-LCN2. (D and E) Evaluation of Garcia score and Beam balance score in ICH rats after injection of Lv-LCN2. (F) Pathological examination using HE staining after knockdown of LCN2 (magnification 20×). Arrows indicate inflammatory cells. (G) Co-staining of TUNEL and NEUN for apoptotic neurons in brain tissues after knockdown of LCN2. (magnification 20×). \*\**P* < 0.01 and \*\*\**P* < 0.0001, versus sham group. #*P* < 0.05, ##*P* < 0.01 and ###*P* < 0.0001, versus Lv-NC group.

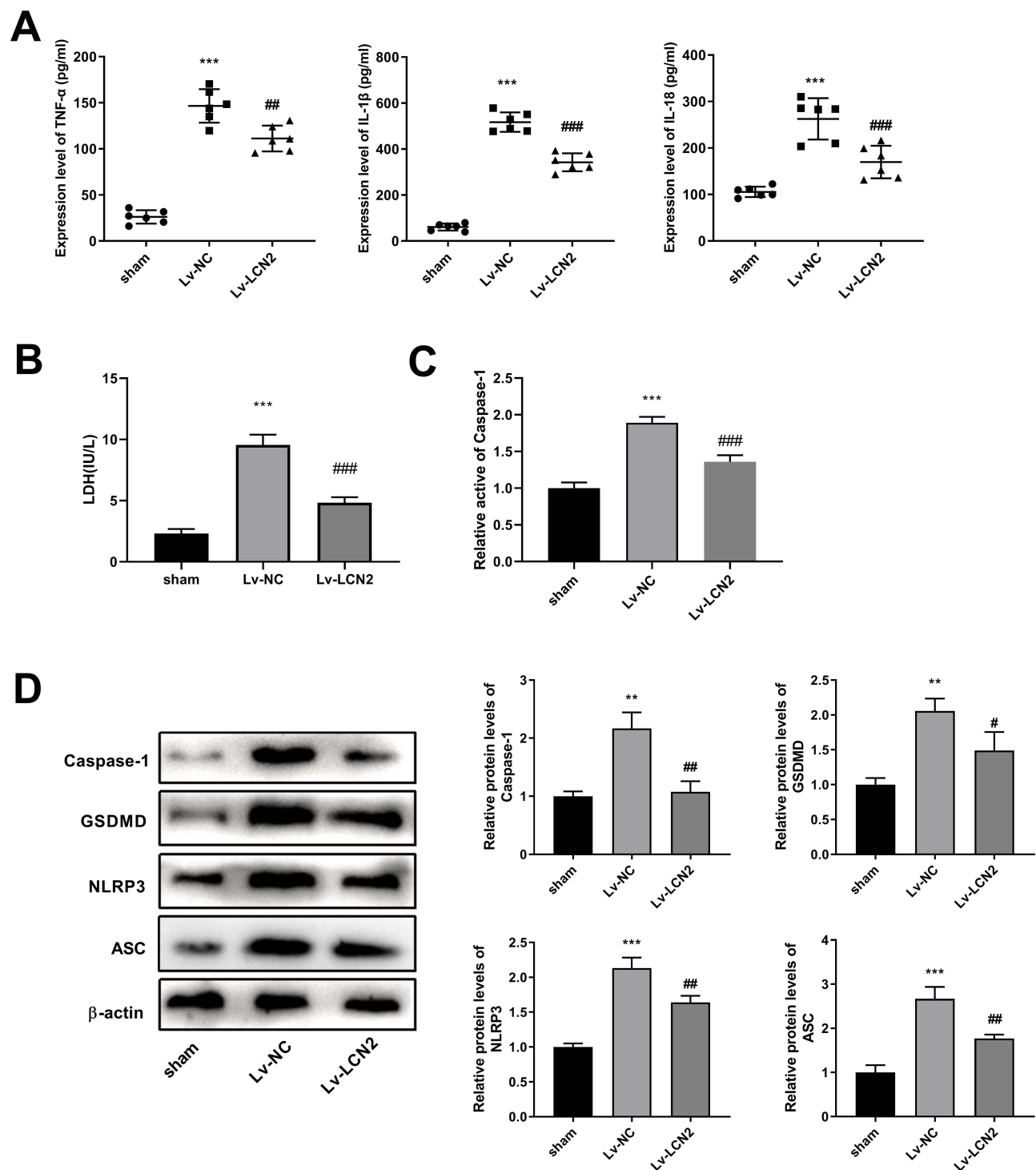


**Figure 7** Knockdown of LCN2 suppresses pyroptosis in ICH rats.

**Notes:** (A) The expression levels of pro-inflammatory cytokines TNF- $\alpha$ , IL-1 $\beta$ , and IL-18 in brain tissues after knockdown of LCN2 measured by ELISA. (B) LDH content was measured in the sham, Lv-NC, and Lv-LCN2 groups. (C) Caspase-1 activity was assessed after knockdown of LCN2. (D) Protein levels of Caspase-1, GSDMD, NLRP3, and ASC detected in the brain tissues after knockdown of LCN2 using Western blot analysis. \*\* $P < 0.01$  and \*\*\* $P < 0.0001$ , versus sham group. # $P < 0.05$ , ## $P < 0.01$ , ### $P < 0.0001$ , versus Lv-NC group.

LCN2 contributes to peroxiredoxin 2-driven brain swelling, inflammatory response, and neuronal death.<sup>40</sup> As previously depicted, LCN2 is highly expressed in astrocytes under various brain injury conditions, and the astrocytic LCN2 is implicated in neuroinflammation.<sup>41</sup> Secreted LCN2 may have a great impact on peripheral organ functions and

the innate immune system during hypoxic injury in brain.<sup>42</sup> Moreover, LCN2 exacerbates brain injury and iron toxicity with ferritin upregulation after ICH.<sup>43</sup> At present, LCN2 has been considered as a promising therapeutic target for brain injury. Zhao et al have illustrated that the application of Deferoxamine could alleviate brain injury after traumatic ICH through the downregulation of LCN2 in rats.<sup>44</sup> Moreover, transcriptome sequencing has revealed that LCN2 is an upregulated DEG in mice with lung infection after ICH. The herb formula (Ginseng Radix et Rhizoma, Aconiti Lateralis Radix Praeparata, and Cistanches Herba) significantly downregulated LCN2, which suggests that LCN2 serves a potential therapeutic target for ICH-induced complication.<sup>45</sup> In the present investigation, we found that LCN2 was highly expressed in ICH, which was consistent with previous studies. Furthermore, our findings that the knockdown of LCN2 resulted in reduced brain water content and improvement in the Garcia score and Beam balance score, provides additional evidence that the LCN2 suppression mitigates brain injury following ICH.

Inflammasome-mediated pyroptosis is a type of programmed cell death that plays an important role in neuroinflammation.<sup>46</sup> In response to harmful stimuli, cells activate inflammasomes comprising NLRs, ASC, and Caspase-1, ultimately leading to shear-induced Caspase-1 activation. The activated Caspase-1 engages in facilitating IL-1 $\beta$  and IL-18 release and activating the pyroptosis executive protein GSDMD.<sup>15,47</sup> Notably, the trigger of NLRP3 inflammasome serves a regulator of LCN2 production, implying that there is a linkage between inflammasome activation and LCN2 expression in the innate immunity.<sup>16</sup> NLRP3 inflammasome activation and Gasdermin D-driven pyroptosis has been demonstrated as a inducer of not only systemic inflammatory responses but also contribute to local norovirus-induced inflammation, where the secretion of fecal LCN2 is promoted.<sup>48</sup> Previous studies have showed that LCN2 triggers NLRP3 inflammasome activation through HMGB1-mediated TLR4 signaling in heart tissue under pressure overload, and LCN2 has been considered as a pro-inflammatory regulator in murine macrophages.<sup>49,50</sup> These findings shed new insight on the detrimental role of LCN2 and provide a potential therapeutic target for diseases. Su et al have revealed that inhibition of LCN2 alleviates retinal vascular dysfunction through suppressing caspase-1-mediated pyroptosis in diabetes mellitus.<sup>51</sup> Astrocyte pyroptosis induced by LCN2 promotes neuroinflammatory damage through the activation of the NLRP3 inflammasome in cerebral ischemia/reperfusion injury.<sup>52</sup> In this study, further experiments showed that LCN2 knockdown resulted in decreased levels of TNF- $\alpha$ , IL-1 $\beta$ , IL-18, and LDH, along with reduced Caspase-1 activity. Furthermore, LCN2 silencing also reduced protein expression of Caspase-1, NLRP3, GSDMD, and ASC. These results demonstrated that knockdown LCN2 inhibited pyroptosis in ICH, which has rarely been reported previously. Previous study has revealed that by inhibiting pyroptosis, particularly through direct targeting of NLRP3 or its upstream molecules, or by directly interfering with Caspase-1 expression and GSDMD formation, the prognosis of ICH can be significantly improved.<sup>12</sup> Moreover, Didymin inhibits microglia pyroptosis and neuroinflammation by targeting the ASC/Caspase-1/GSDMD pathway after experimental ICH.<sup>53</sup> These results suggest that LCN2 contributes to brain injury after ICH may by regulating pyroptosis, making it a potential therapeutic target for ICH.

Some limitations should be noted in this study. Although we have demonstrated LCN2 serves as a potential biomarker for ICH, the cellular location of LCN2 in sham and ICH rats remains unclarified. Hence, the investigations of cellular distribution of LCN2 after ICH may help deepen our understanding of its role in ICH. Besides, except for LCN2, the regulation of other DEGs (such as Hspb1, CXCL10 and Mef2b) is necessary to be studies to supplement potential mechanism and targets for ICH. Functional enrichment analysis reveals the s significantly enriched pathways for DEGs, which may provide a direction for the mechanism. Therefore, further experiments should be conducted to investigate the underlying mechanism of DEGs, especially for LCN2.

## Conclusion

In summary, we identified 103 significantly upregulated and 81 downregulated DEGs in ICH rats, among which LCN2 was upregulated after ICH. Furthermore, experimental studies revealed that knockdown LCN2 attenuated brain injury after ICH. Mechanically, suppression of LCN2 led to a reduction in TNF- $\alpha$ , IL-1 $\beta$ , IL-18, and LDH levels, accompanied by a decrease in Caspase-1 activity. Additionally, silencing of LCN2 resulted in lowered protein expression of Caspase-1, NLRP3, GSDMD, and ASC in the ICH model, which suggested that LCN2 knockdown might improve brain injury after ICH by inhibiting pyroptosis. These results facilitate the underlying regulatory role of LCN2 in ICH and provide promising target for ICH management.

## Data Sharing Statement

The datasets generated and/or analysed during the current study are available in the [NCBI] repository, [<http://www.ncbi.nlm.nih.gov/bioproject/952712>].

## Ethical Approval and Consent to Participate

All methods are reported in accordance with ARRIVE guidelines for the reporting of animal experiments. The animal experiments conformed to the Guide for the Care and Use of Laboratory Animals. Animal study has been approved by the Animal Ethics Committee of The First Affiliated Hospital of Gannan Medical University. All methods were performed in accordance with Declaration of Helsinki.

## Author Contributions

All authors made a significant contribution to the work reported, whether that is in the conception, study design, execution, acquisition of data, analysis and interpretation, or in all these areas; took part in drafting, revising or critically reviewing the article; gave final approval of the version to be published; have agreed on the journal to which the article has been submitted; and agree to be accountable for all aspects of the work.

## Funding

Jiangxi Provincial Health Committee (202130622, 20201088); Ganzhou Science and Technology Project (GZ2021ZSF060, GZ2016ZSF206).

## Disclosure

The authors declare that they have no conflicts of interest to disclose.

## References

1. Unnithan AKA, Mehta P. Hemorrhagic stroke; 2020.
2. Ziai WC, Carhuapoma JR. Intracerebral hemorrhage. *Continuum*. 2018;24(6):1603–1622.
3. Shao Z, Tu S, Shao A. Pathophysiological mechanisms and potential therapeutic targets in intracerebral hemorrhage. *Front Pharmacol*. 2019;10:1079. doi:10.3389/fphar.2019.01079
4. McKenzie BA, Dixit VM, Power C. Fiery cell death: pyroptosis in the central nervous system. *Trends Neurosci*. 2020;43(1):55–73. doi:10.1016/j.tins.2019.11.005
5. Zhaolin Z, Guohua L, Shiyuan W, Zuo W. Role of pyroptosis in cardiovascular disease. *Cell Proliferation*. 2019;52(2):e12563. doi:10.1111/cpr.12563
6. Luo Q, Shi X, Ding J, et al. Network pharmacology integrated molecular docking reveals the antiosteosarcoma mechanism of biochanin A. *Evid Based Complement Alternat Med*. 2019;2019:1410495.
7. Wu J, Lin S, Wan B, Velani B, Zhu Y. Pyroptosis in liver disease: new insights into disease mechanisms. *Aging Dis*. 2019;10(5):1094. doi:10.14336/AD.2019.0116
8. Fang Y, Tian S, Pan Y, et al. Pyroptosis: a new frontier in cancer. *Biomed Pharmacother*. 2020;121:109595.
9. Hu Y, Wang B, Li S, Yang S. Pyroptosis, and its role in central nervous system disease. *J Mol Biol*. 2022;434(4):167379.
10. Shi M, Chen J, Liu T, et al. Protective effects of remimazolam on cerebral ischemia/reperfusion injury in rats by inhibiting of NLRP3 inflammasome-dependent pyroptosis. *Drug Des Devel Ther*. 2022;16:413. doi:10.2147/DDDT.S344240
11. Yin K, Lu H, Zhang Y, et al. Secondary brain injury after polystyrene microplastic-induced intracerebral hemorrhage is associated with inflammation and pyroptosis. *Chem Biol Interact*. 2022;367:110180. doi:10.1016/j.cbi.2022.110180
12. Song D, Yeh C-T, Wang J, Guo F. Perspectives on the mechanism of pyroptosis after intracerebral hemorrhage. *Front Immunol*. 2022;13. doi:10.3389/fimmu.2022.989503
13. Chen G, Gao C, Yan Y, et al. Inhibiting Er stress weakens neuronal pyroptosis in a mouse acute hemorrhagic stroke model. *Mol Neurobiol*. 2020;57(12):5324–5335. doi:10.1007/s12035-020-02097-9
14. Li X, Wang T, Zhang D, et al. Andrographolide ameliorates intracerebral hemorrhage induced secondary brain injury by inhibiting neuroinflammation induction. *Neuropharmacology*. 2018;141:305–315. doi:10.1016/j.neuropharm.2018.09.015
15. Lin X, Ye H, Siaw-Debrah F, et al. AC-YVAD-CMK inhibits pyroptosis and improves functional outcome after intracerebral hemorrhage. *Biomed Res Int*. 2018;2018:1–10. doi:10.1155/2018/3706047
16. Ahn H, Lee G, Kim J, et al. NLRP3 triggers attenuate lipocalin-2 expression independent with inflammasome activation. *Cells*. 2021;10(7):1660. doi:10.3390/cells10071660
17. Yang W-S, Shen Y-Q, Yang X, et al. MicroRNA transcriptomics analysis identifies dysregulated hedgehog signaling pathway in a mouse model of acute intracerebral hemorrhage exposed to hyperglycemia. *J Stroke Cerebrovascular Dis*. 2022;31(3):106281. doi:10.1016/j.jstrokecerebrovasdis.2021.106281
18. Al Jaber S, Cohen A, D'Souza C, et al. Lipocalin-2: structure, function, distribution and role in metabolic disorders. *Biomed Pharmacother*. 2021;142:112002. doi:10.1016/j.biopha.2021.112002

19. Tang W, Ma J, Gu R, Lei B, Ding X, Xu G. Light-induced lipocalin 2 facilitates cellular apoptosis by positively regulating reactive oxygen species/Bim signaling in retinal degeneration. *Invest Ophthalmol Visual Sci.* 2018;59(15):6014–6025. doi:10.1167/iovs.18-25213
20. Shin HJ, Jeong EA, Lee JY, et al. Lipocalin-2 deficiency reduces oxidative stress and neuroinflammation and results in attenuation of kainic acid-induced hippocampal cell death. *Antioxidants.* 2021;10(1):100. doi:10.3390/antiox10010100
21. Hu C, Yang K, Li M, Huang W, Zhang F, Wang H. Lipocalin 2: a potential therapeutic target for breast cancer metastasis. *Onco Targets Ther.* 2018;11:8099. doi:10.2147/OTT.S181223
22. Dekens DW, Eisel UL, Gouweleuw L, Schoemaker RG, De Deyn PP, Naudé PJ. Lipocalin 2 as a link between ageing, risk factor conditions and age-related brain diseases. *Ageing Res Rev.* 2021;70:101414. doi:10.1016/j.arr.2021.101414
23. Llorens F, Hermann P, Villar-Piqué A, et al. Cerebrospinal fluid lipocalin 2 as a novel biomarker for the differential diagnosis of vascular dementia. *Nat Commun.* 2020;11(1):1–11. doi:10.1038/s41467-020-14373-2
24. Song J, Kim OY. Perspectives in Lipocalin-2: emerging biomarker for medical diagnosis and prognosis for Alzheimer's disease. *Clin Nutr Res.* 2018;7(1):1–10. doi:10.7762/cnr.2018.7.1.1
25. Luo C, Zhou S, Yin S, et al. Lipocalin-2 and cerebral stroke. *Front Mol Neurosci.* 2022;2022:15.
26. Liu L, Wang S, Xu R, et al. Experimental intracerebral haemorrhage: description of a semi-coagulated autologous blood model in rats. *Neurological Res.* 2015;37(10):874–879. doi:10.1179/1743132815Y0000000067
27. Guo Q, Xie M, Guo M, Yan F, Li L, Liu R. ZEB2, interacting with MDM2, contributes to the dysfunction of brain microvascular endothelial cells and brain injury after intracerebral hemorrhage. *Cell Cycle.* 2021;20(17):1692–1707. doi:10.1080/15384101.2021.1959702
28. Matsumura K, Kumar TP, Guddanti T, Yan Y, Blackburn SL, McBride DW. Neurobehavioral deficits after subarachnoid hemorrhage in mice: sensitivity analysis and development of a new composite score. *J Am Heart Assoc.* 2019;8(8):e011699. doi:10.1161/JAHA.118.011699
29. Ren H, Han R, Chen X, et al. Potential therapeutic targets for intracerebral hemorrhage-associated inflammation: an update. *J Cereb Blood Flow Metab.* 2020;40(9):1752–1768. doi:10.1177/0271678X20923551
30. Fei X, He Y, Chen J, et al. The role of toll-like receptor 4 in apoptosis of brain tissue after induction of intracerebral hemorrhage. *J Neuroinflammation.* 2019;16(1):1–14. doi:10.1186/s12974-019-1634-x
31. Zhang X, Wu Y, Wang D, Jin X, Li C. Expression changes of inflammatory cytokines TNF- $\alpha$ , IL-1 $\beta$  and HO-1 in hematoma surrounding brain areas after intracerebral hemorrhage. *J Biol Regul Homeost Agents.* 2019;33(5):1359–1367. doi:10.23812/19-150-A
32. Li W, Liu X, Tu Y, et al. Dysfunctional Nurr1 promotes high glucose-induced Müller cell activation by up-regulating the NF- $\kappa$ B/NLRP3 inflammasome axis. *Neuropeptides.* 2020;82:102057. doi:10.1016/j.npep.2020.102057
33. Ding H, Li Y, Wen M, Liu X, Han Y, Zeng H. Elevated intracranial pressure induces IL-1 $\beta$  and IL-18 overproduction via activation of the NLRP3 inflammasome in microglia of ischemic adult rats. *Int J Mol Med.* 2021;47(1):183–194. doi:10.3892/ijmm.2020.4779
34. Ma Q, Chen S, Hu Q, Feng H, Zhang JH, Tang J. NLRP3 inflammasome contributes to inflammation after intracerebral hemorrhage. *Ann Neurol.* 2014;75(2):209–219. doi:10.1002/ana.24070
35. Liang Y, Song P, Chen W, et al. Inhibition of caspase-1 ameliorates ischemia-associated blood-brain barrier dysfunction and integrity by suppressing pyroptosis activation. *Front Cell Neurosci.* 2021;14:540669. doi:10.3389/fncel.2020.540669
36. Gu L, Sun M, Li R, et al. Activation of RKIP binding ASC attenuates neuronal pyroptosis and brain injury via Caspase-1/GSDMD Signaling pathway after intracerebral hemorrhage in mice. *Transl Stroke Res.* 2022;1–18. doi:10.1007/s12975-021-00927-z
37. Liu Z, Zhang R, Chen X, et al. Identification of hub genes and small-molecule compounds related to intracerebral hemorrhage with bioinformatics analysis. *PeerJ.* 2019;7:e7782.
38. Chen S, Zhao L, Sherchan P, et al. Activation of melanocortin receptor 4 with RO27-3225 attenuates neuroinflammation through AMPK/JNK/p38 MAPK pathway after intracerebral hemorrhage in mice. *J Neuroinflammation.* 2018;15(1):1–13. doi:10.1186/s12974-018-1140-6
39. Chen Y, Dong J, Yang D, et al. Synergistic network pharmacology for traditional Chinese medicine liangxue tongyu formula in acute intracerebral hemorrhagic stroke. *Neural Plast.* 2021;2021:1–21. doi:10.1155/2021/8874296
40. Zhang J, Novakovic N, Hua Y, Keep RF, Xi G. Role of lipocalin-2 in extracellular peroxiredoxin 2-induced brain swelling, inflammation and neuronal death. *Exp Neurol.* 2021;335:113521. doi:10.1016/j.expneurol.2020.113521
41. Suk K. Lipocalin-2 as a therapeutic target for brain injury: an astrocentric perspective. *Prog Neurobiol.* 2016;144:158–172. doi:10.1016/j.pneurobio.2016.08.001
42. Ranjbar Taklimie F, Gasterich N, Scheld M, et al. Hypoxia induces astrocyte-derived lipocalin-2 in ischemic stroke. *Int J Mol Sci.* 2019;20(6):1271. doi:10.3390/ijms20061271
43. Ni W, Zheng M, Xi G, Keep RF, Hua Y. Role of lipocalin-2 in brain injury after intracerebral hemorrhage. *J Cereb Blood Flow Metab.* 2015;35(9):1454–1461. doi:10.1038/jcbfm.2015.52
44. Zhao J, Xi G, Wu G, Keep RF, Hua Y. *Deferoxamine Attenuated the Upregulation of Lipocalin-2 Induced by Traumatic Brain Injury in Rats.* Brain Edema XVI: Springer; 2016:291–294.
45. Miao Y, Wang B, Hu J, et al. Herb formula (GCis) prevents pulmonary infection secondary to intracerebral hemorrhage by enhancing peripheral immunity and intestinal mucosal immune barrier. *Front Pharmacol.* 2022;13:1.
46. Ding R, Li H, Liu Y, et al. Activating cGAS–STING axis contributes to neuroinflammation in CVST mouse model and induces inflammasome activation and microglia pyroptosis. *J Neuroinflammation.* 2022;19(1):137. doi:10.1186/s12974-022-02511-0
47. Jian D, Qin L, Gan H, et al. NPAS4 exacerbates pyroptosis via transcriptionally regulating NLRP6 in the acute phase of intracerebral hemorrhage in mice. *Int J Mol Sci.* 2023;24(9):8320. doi:10.3390/ijms24098320
48. Dubois H, Sorgeloos F, Sarvestani ST, et al. Nlrp3 inflammasome activation and Gasdermin D-driven pyroptosis are immunopathogenic upon gastrointestinal norovirus infection. *PLoS Pathogens.* 2019;15(4):e1007709. doi:10.1371/journal.ppat.1007709
49. Song E, Jahng JW, Chong LP, et al. Lipocalin-2 induces NLRP3 inflammasome activation via HMGB1 induced TLR4 signaling in heart tissue of mice under pressure overload challenge. *Am J Transl Res.* 2017;9(6):2723.
50. Kim SL, Shin MW, Kim SW. Lipocalin 2 activates the NLRP3 inflammasome via LPS-induced NF- $\kappa$ B signaling and plays a role as a pro-inflammatory regulator in murine macrophages. *Mol Med Rep.* 2022;26(6):1–10. doi:10.3892/mmr.2022.12875
51. Su X, Zhou P, Qi Y. Down-regulation of LCN2 attenuates retinal vascular dysfunction and caspase-1-mediated pyroptosis in diabetes mellitus. *Ann Translat Med.* 2022;10(12):695. doi:10.21037/atm-22-2655

52. Li J, Xu P, Hong Y, et al. Lipocalin-2-mediated astrocyte pyroptosis promotes neuroinflammatory injury via NLRP3 inflammasome activation in cerebral ischemia/reperfusion injury. *J Neuroinflammation*. 2023;20(1):148. doi:10.1186/s12974-023-02819-5
53. Gu L, Sun M, Li R, et al. Didymin suppresses microglia pyroptosis and neuroinflammation through the Asc/Caspase-1/GSDMD pathway following experimental intracerebral hemorrhage. *Front Immunol*. 2022;13:810582. doi:10.3389/fimmu.2022.810582

### Neuropsychiatric Disease and Treatment

Dovepress

### Publish your work in this journal

Neuropsychiatric Disease and Treatment is an international, peer-reviewed journal of clinical therapeutics and pharmacology focusing on concise rapid reporting of clinical or pre-clinical studies on a range of neuropsychiatric and neurological disorders. This journal is indexed on PubMed Central, the 'PsycINFO' database and CAS, and is the official journal of The International Neuropsychiatric Association (INA). The manuscript management system is completely online and includes a very quick and fair peer-review system, which is all easy to use. Visit <http://www.dovepress.com/testimonials.php> to read real quotes from published authors.

Submit your manuscript here: <https://www.dovepress.com/neuropsychiatric-disease-and-treatment-journal>